



RESEARCH ARTICLE

A comparison of gold and silver nanocones and geometry optimisation for tip-enhanced microscopy

Luke R. McCourt¹ | Michael G. Ruppert¹ | Ben S. Routley¹ |
Sathish C. Indirathankam² | Andrew F. Fleming¹

¹School of Electrical Engineering and Computer Science, The University of Newcastle, Newcastle, New South Wales, 2308, Australia

²Global Innovative Centre for Advanced Nanomaterials, The University of Newcastle, Newcastle, New South Wales, 2308, Australia

Correspondence

Luke McCourt, School of Electrical Engineering and Computer Science, The University of Newcastle, Newcastle, New South Wales, 2308, Australia.
Email: Luke.Mccourt@uon.edu.au

Abstract

In this article, boundary element method simulations are used to optimise the geometry of silver and gold nanocone probes to maximise the localised electric field enhancement and tune the near-field resonance wavelength. These objectives are expected to maximise the sensitivity of tip-enhanced Raman microscopes. Similar studies have used limited parameter sets or used a performance metric other than localised electric field enhancement. In this article, the optical responses for a range of nanocone geometries are simulated for excitation wavelengths ranging from 400 to 1000 nm. Performance is evaluated by measuring the electric field enhancement at the sample surface with a resonant illumination wavelength. These results are then used to determine empirical models and derive optimal nanocone geometries for a particular illumination wavelength and tip material. This article concludes that gold nanocones are expected to provide similar performance to silver nanocones at red and near-infrared wavelengths, which is consistent with other results in the literature. In this article, 633 nm is determined to be the shortest usable illumination wavelength for gold nanocones. Below this limit, silver nanocones will provide superior enhancement. The use of gold nanocone probes is expected to dramatically improve probe lifetime, which is currently measured in hours for silver coated probes. Furthermore, the elimination of passivation coatings is expected to enable smaller probe radii and improved topographical resolution.

KEY WORDS

nano-antenna, nanocone, near-field enhancement, tip-enhanced raman spectroscopy (TERS)

1 | INTRODUCTION

Currently available probes for near-field applications consist of a silicon atomic force microscope (AFM) tip with a thick silver coating. They generally suffer from inconsistent performance, low topographic resolution and an offset between the Raman signal and topological map.^[1] Furthermore, the silver rapidly tarnishes in ambient conditions resulting in lifetimes of approximately

1 day.^[2] Alternate probes consisting of a metal nanocone attached to a silicon AFM tip have been produced,^[3] which will likely offer more consistent performance and superior topographic resolution. The near-field resonance wavelength and localised electric field enhancement of these nanocone probes is yet to be accurately modelled. In this article, boundary element method (BEM) simulations are used to calculate the near-field resonance wavelength and electric field enhancement of nanocone tips

and map the dependencies of tip dimensions and material. The aim of this work is to produce numerical models that describe the optimal geometry of gold and silver nanocones for excitation wavelengths from the visible to near-infrared. Gold nanocones have a longer lifetime than silver nanocones due to the chemical stability, and therefore, it is of interest to identify the wavelength range where the performance is comparable with silver.

The diffraction limit determines the maximum resolution of microscopy techniques. The diffraction limit can be overcome using the optical near-field that consists of electric and magnetic fields that are strongly localised to a surface or narrow aperture.^[4] The electric field localisation allows higher resolutions to be achieved compared with using far-field light. Furthermore, the spatial confinement is wavelength independent, allowing long wavelength illumination sources to be used.^[5]

The method of near-field production considered here is to excite a localised surface plasmon resonance (LSPR) that is resonant oscillations of conduction electrons on the surface of a nanoparticle or an ensemble of nanoparticles.^[6] This results in a near field consisting of electric and magnetic fields strongly confined to the surface.^[7]

Tip-enhanced Raman spectroscopy (TERS) is an imaging technique that makes use of the near-field generated through LSPRs.^[8] Similar to far-field Raman spectroscopy, the wavelength shift between the illumination source and scattered light gives chemical information about the sample. Compared with Raman spectroscopy, TERS significantly increases the spatial resolution due to the tight spatial confinement of the near field. This is illustrated in Figure 1 where a LSPR on a nanoparticle can be used for tip-enhanced near-field applications. A focussed laser beam excites a LSPR on a metallic nanoparticle located at the end of an AFM tip. The near field increases the interaction with the sample in close proximity to the tip only. As a result, TERS has been used to demonstrate single molecule Raman responses on a variety of samples.^[6,9] Increased mapping speeds are likely to come from improved AFM cantilevers in the near future.^[10]

The near field can also be used to induce chemical reactions in a substrate for photolithography. Feature sizes as low as one-tenth of the excitation wavelength (well below the diffraction limit) have been achieved using the near field from an AFM tip to induce polymerisation.^[11] This represents a significant improvement in resolution compared with far-field maskless lithography that is diffraction limited.^[12]

For an LSPR to form, the particle has to be spatially confined in all three dimensions. Furthermore, the particle material needs to have a negative real permittivity and a low imaginary permittivity, which damps

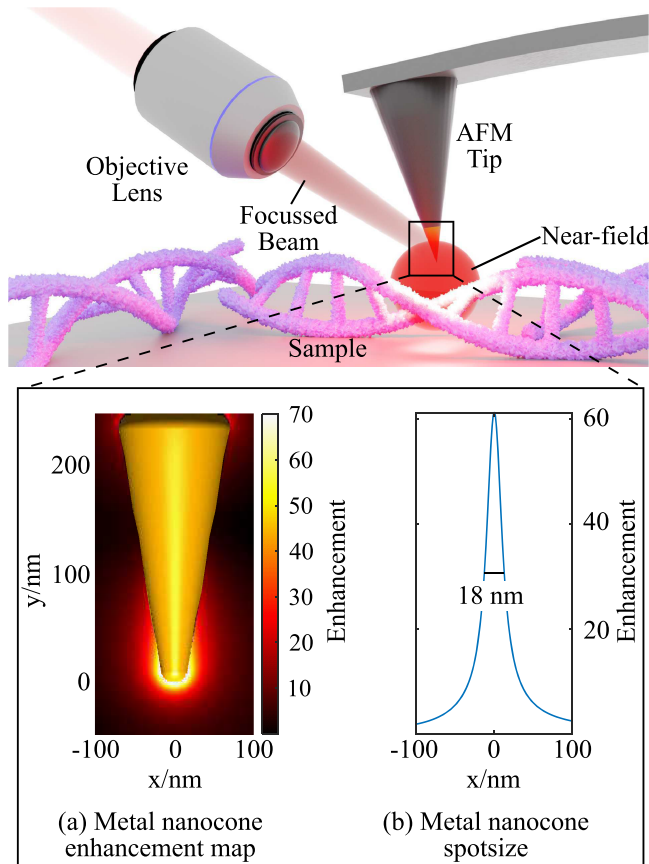


FIGURE 1 Illustration of basic operating principle of apertureless near-field applications where a laser is focussed onto a plasmonically active metallic tip. This produces a near-field that is kept in close proximity to the sample using an AFM system, resulting in increased Raman scattering for tip-enhanced Raman spectroscopy (TERS) or increased photoresist exposure for lithography. (a) Simulated electric field enhancement for a gold nanocone. (b) Electric field enhancement 1 nm below gold nanocone with the spot size (full width half maximum) showing the spatial confinement of the field (black line). AFM, atomic force microscope

LSPRs.^[7] Examples of such materials are silver and gold. In addition, LSPR wavelength is dependent upon material permittivity and particle geometry.^[13] Hence, probe geometry needs to be adjusted so an LSPR exists at the illumination wavelength.

The current industry standard tip for near-field applications consists of a silicon AFM tip with a silver coating, which forms a grainy surface. A scanning electron microscope image of one such tip is shown in Figure S1. The discrete metal grains provide particle confinement, and silver meets the permittivity requirements, most notably having low loss across the visible spectrum.^[14] However, there are a number of disadvantages associated with these probes. First, the random nature of grain formation^[15,16] results in inconsistent electric field enhancement and near-field resonance wavelength. Second, to

ensure a nanoparticle at the tip apex, a thick metal coating is required, which decreases optical and topographic resolution. For the tip shown in Figure S1, the apex radius of 45 nm will result in an optical resolution of approximately 90 nm. Third, there is often an issue with collocation, where the enhanced near field is not located at the AFM tip apex. In the case of TERS, this results in an offset between Raman and topography maps.^[1] Finally, silver nanoparticles tarnish rapidly in laboratory conditions, exhibiting a decreased absorption coefficient by one order of magnitude over 36 h and a redshifting near-field resonance wavelength of 1.8 nm/h.^[2] Thus, silver-based tips have lifetimes limited to approximately 1 day, which is prohibitive given the significant set-up time associated with aligning the optical system that must be performed for each new tip. To extend the lifetime, a passivation layer may be added. However, this increases the separation between the plasmonically active silver and the sample resulting in decreased near-field enhancement, optical and topographic resolutions.

An alternative tip consists of a metallic nanocone attached to the end of a silicon AFM probe. This design is illustrated in Figure 1, with the electric field enhancement surrounding the gold nanocone in Figure 1a and the enhancement perpendicular to the cone axis, below the apex, shown in Figure 1b. These nanocones can be manufactured using focussed ion beam milling with consistent surface topologies, producing more consistent electric field enhancement and near-field resonance wavelengths.^[3] In addition, the nanocone apex is both the source of near-field enhancement and mechanical apex removing the collocation issue. Furthermore, these nanocones can be produced with apex radii of approximately 10 nm, providing superior optical and mechanical resolution to commercially available silver-coated tips. Finally, nanocone geometry can be altered to shift the LSPR to the excitation wavelength,^[13] allowing the use of alternative materials with higher chemical stability than silver.

As nanoparticle material and geometry affect the LSPR wavelength and near-field enhancement, the material and shape of the nanocone tips need to be optimised for a required optical wavelength. In contrast to spheres and ellipsoids, no analytic solutions for the optical response of nanocones exist.^[7] Hence, computational methods are needed to optimise nanocone geometry.

Previous studies have investigated the optical performance of geometries similar to the nanocone considered here. However, some have only considered a single excitation wavelength^[6,17-20] that does not allow the near-field resonance wavelength and peak enhancement to be identified. Others use quantities other than near-field enhancement such as optical extinction^[6,21] or antenna efficiency.^[22] However, simulation allows direct

calculation of electric field enhancement and the effects of material and geometry to be investigated. Furthermore, by considering limited nanocone geometry parameters, studies have failed to produce generalised models of near-field resonance wavelength and enhancement in the visible spectrum.^[23,24]

2 | CONTRIBUTIONS

In this work, detailed simulations of the electric field enhancement below the tip apex are provided. The BEM is employed to calculate electric field enhancement for a wide range of nanocone geometries and excitation beam wavelengths. Compared with previous studies that consider only a small number of geometries or a fixed illumination wavelength, this work computes the enhancement for every feasible combination of geometry and illumination wavelength, with sufficient wavelength resolution to identify the spectral peak for each geometry. This approach allows the derivation of optimal nanocone material and geometry combinations for wavelengths commonly used in near-field applications. The results predict that gold will achieve similar enhancement to silver at red and near-infrared wavelengths. Therefore, gold nanocone tips with improved chemical stability and lifetime are concluded to be feasible.

3 | METHOD

3.1 | Tip performance metrics

Two metrics for tip performance are used throughout this work. First, the electric field enhancement, referred to as ‘enhancement’, is $E_{\text{enh}} = E_{\text{res}}/E_{\text{exc}}$, where E_{res} is the maximum electric field strength in the plane 1 nm below the sample surface, perpendicular to the cone axis, and E_{exc} is the electric field strength of the excitation beam, which is set to 1 V/m. A high enhancement is desirable as the ratio of near-field to far-field increases. An example electric field map for a nanocone is plotted in Figure 1a. The second metric, spot size, is the full width half maximum of the electric field in the plane 1 nm below the sample surface, perpendicular to the cone axis. A smaller spot size improves resolution in near-field applications. An example spot size calculation is illustrated in Figure 1b.

3.2 | BEM simulations

The BEM package, metallic nanoparticles using BEM (MNPBEM),^[25,26] was used to solve Maxwell's equations in the frequency domain for gold and silver metallic

nanocone structures above a lossless glass substrate. The problem space is described in Figure 2. The particle boundaries consist of boundary elements that are defined by a set of vertex positions and normal vectors. Measured dielectric functions^[27] for gold or silver were used inside the boundary. The substrate was assumed to be a lossless material with a refractive index of 1.5, approximating glass. A plane wave excitation E_{exc} was used, propagating in x with y polarisation, a configuration that has been shown to maximise enhancement.^[20] Particle geometry was varied using combinations of particle length L , radius of curvature r and apex angle θ .

For each tip geometry, the near-field resonance wavelength was identified by the maximum electric field enhancement. The order of each mode was identified from the surface charge distribution, with the order corresponding to the number of zero surface charge nodes in \hat{y} . Examples of first- and second-order longitudinal modes are shown in Figure S2. For consistency, only results for the first-order mode are given for each nanocone.

4 | RESULTS AND DISCUSSION

4.1 | Nanocone parameters

For nanocones of silver and gold located 1 nm ($s = 1 \text{ nm}$) above a glass substrate, the near-field resonance wavelength was identified, and the enhancement at this wavelength calculated 1 nm below the glass surface (a total of 2 nm below the tip apex). The results of this are shown in

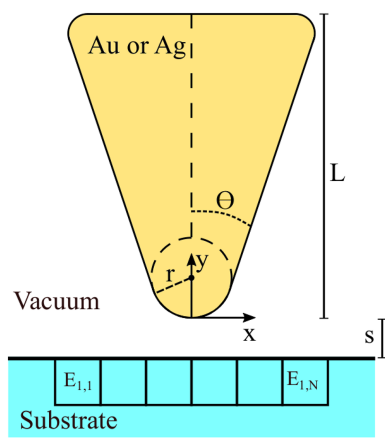


FIGURE 2 x-y cross section of the simulation problem space, consisting of a vacuum with an embedded nanocone tip defined by an outer boundary with length L , radius of curvature r and apex angle θ . The tip is positioned with the bottom vertex at the origin, separated a distance s above a substrate of 1.5 refractive index. Electric field values are calculated over an $1 \times N$ grid located 1 nm below the substrate surface

Figure 3 with each data point representing a unique nanocone geometry defined by the radius, angle and length on the xyz axis. Figure 3a shows the near-field resonance wavelength for silver nanocones. Enhancement spectra for the boxed data points, A1–A4, are shown. The enhancement achieved at the near-field resonance wavelength of each silver nanocone is shown in Figure 3b, and the enhancement spectra for the boxed data points, B1–B4, are shown. Similarly, the near-field resonance wavelengths and corresponding enhancements for gold nanocones are shown in Figure 3, panels c and d, respectively. An empirical model can then be used to describe the near-field resonance wavelength and enhancement as a function of length, half angle and radius, in the range of interest.

Fitting a linear regression model using a least squares algorithm to the near-field resonance wavelength data yields

$$\lambda_{\text{res}} (\text{nm}) = \begin{cases} 610 + 1.5L - 7.1\theta + 0.3r, & \text{Gold} \\ 460 + 1.9L - 7.0\theta + 1.1r, & \text{Silver,} \end{cases} \quad (1)$$

where λ_{res} is the near-field resonance wavelength in nm, the radius is in nm and the angle is in degrees. This fit allows for accurate predictions of the near-field resonance wavelength with less than 5% error for both materials when compared with the simulated results. The coefficients reveal that increased length or apex radius induce a redshift of the near-field resonance wavelength, whereas increased angle produces a blueshift. There is a trend where larger radii cause a blueshift for short nanocones, but a redshift for long nanocones. This averages to a slight redshift as radius increases. However, the shifts due to radius are small compared with the shifts associated with length and angle, especially given the small range of radii considered here (5–30 nm).

In addition, the near-field resonance wavelength of gold is 150 nm longer than silver with the same geometry. As a result, even when short nanocones are used, the near-field resonance wavelength of gold nanocones cannot be realistically tuned below 630 nm.

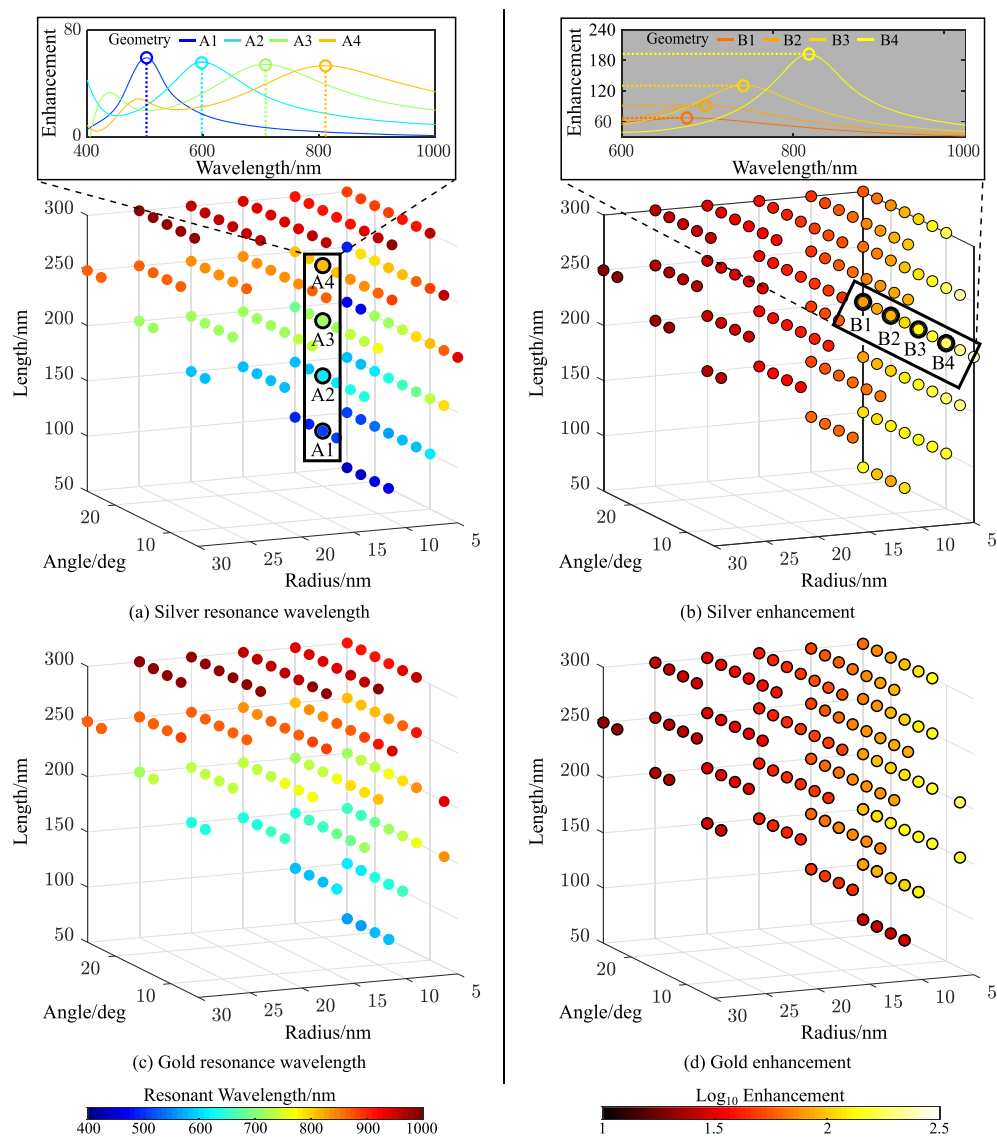
A non-linear optimisation was used to determine the following enhancement models:

$$E_{\text{enh}} = c_1 e^{-2\gamma} + c_2, \quad (2)$$

where c_1 is 770 and 930, and c_2 is 27 and 32 for gold and silver respectively and $\gamma = (r\theta)^{1/2}$ where r is in nm and θ is in radians. The models capture the trend well with a root mean squared error (RMSE) in enhancement of 12.

The enhancement models are shown (Equation 2), together with the simulated enhancements in Figure 4.

FIGURE 3 The simulated optical responses of silver and gold nanocones 1 nm above a glass substrate, measured 1 nm below the glass surface are given with example spectra in the top plots. (a) Silver and (c) gold show the near-field resonance wavelengths of nanocones. The wavelength scale is in the bottom left. The near-field resonance wavelength is redshifted when moving to longer lengths and smaller angles. (b) Silver and (d) gold show the electric field enhancement of nanocones. The enhancement scale is in the bottom right. A high enhancement can be observed for nanocones with small radii and cone angles



Enhancement is increased when tip apex angle and radius are small, in effect when the tip is sharp. This differs from hemispherical ellipses where enhancement is dependent on the short to long axis ratio.^[19,28] Equation (2) is length independent, which indicates an increased tip length does not decrease the enhancement at least across the particle lengths considered here and when restricted to the first order longitudinal mode.

Gold nanocones have been manufactured in McMahon et al.,^[3] where the length and far-field scatter resonance wavelengths were measured, whereas a range of cone angles is given. In Figure 5, the near-field resonance wavelength model for gold nanocones (Equation 1) is compared with this experimental data. Probable bounds on the experimental cone angle give a range of near-field resonance wavelengths for a given nanocone length. The model fits the data well, with 4% of the data points falling outside of the models predictions.

This indicates the simulated data and subsequent linear regression model are valid. A particular near-field resonance is typically redshifted from the same resonance observed in the far-field due to retardation effects that become significant as particle size approaches the excitation wavelength.^[29,30] In this study, the particle widths are small compared with the near-field resonance wavelengths; hence, there will be a small shift between the near-field and far-field resonances. Furthermore, the experimental data^[3] measure nanocones terminated on a glass substrate that will redshift the resonance wavelengths as discussed in Section 4.2. This limits the validity of a direct comparison between the experimental data^[3] and the data acquired through simulations. However, due to a lack of experimental near-field resonance data for gold nanocones, this was necessary.

The empirical functions that describe trends in the resonance wavelength and enhancement provide a starting point for the tip design process. The desirable

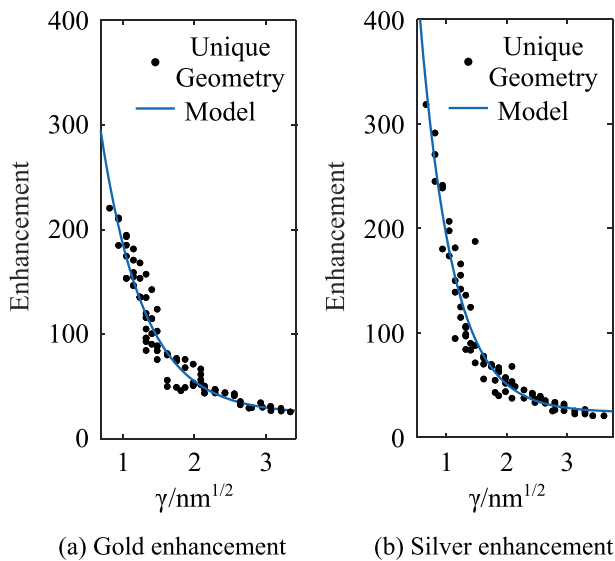


FIGURE 4 The enhancement of each nanocone geometry is plotted as a function of γ (black) for (a) gold and (b) silver. Each data point represents a unique nanocone geometry. The enhancement model (Equation 2) is overlaid (blue) and captures the data well. The highest enhancements occur when γ is small or the nanocone is ‘sharp’.

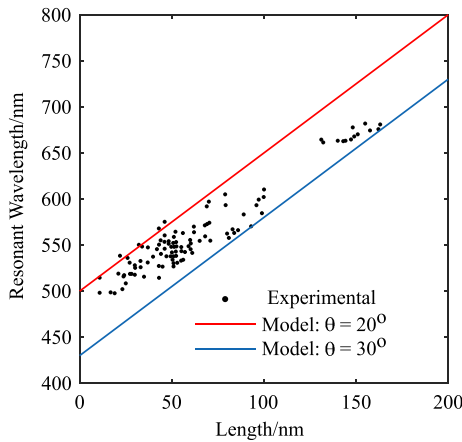


FIGURE 5 The experimental far-field resonance wavelength for gold nanocones (black)^[13] is plotted and compared with the near-field resonance wavelength model (Equation 1). Estimates for maximum and minimum cone angle were chosen as 30° and 20° and radius kept at 10 nm, resulting in upper (blue) and lower (red) estimates from the model, respectively.

characteristics of small spot size and high enhancements are most closely associated with a small tip radius combined with a small tip angle; therefore, these should be minimised within the limits of the available manufacturing process.

Then, the resonance wavelength can be tuned with nanocone length. Optimised length and material combinations are given in Table 1 for commonly used wavelengths in TERS.

Figure 6 shows the spot size as a function of radius, with a single linear fit capturing both the silver and gold data set. Multiple data points at a given radius are for different combinations of length and apex angle; however, the position of these data points within a group could not be predicted. The spot size was found to be independent of length, apex angle and material (gold or silver), with the apex radius being the only strong predictor. The spot size being proportional to radius is consistent with previous results,^[5,31] and so the radius should be minimised.

As gold has a relatively low imaginary permittivity, it provides similar near-field enhancement to silver, provided the geometry is appropriate, and offers the same resolution capabilities. Due to superior corrosion resistance, gold nanocone tips appear to be better suited for imaging and lithography applications in the 633–900 nm wavelength range. Outside of this range, the comparatively low enhancement may limit their use.

It is worth noting that an increased substrate refractive index will result in a redshifted nanocone near-field resonance.^[32] Hence, the wavelength ranges suggested here are limited to use with substrates similar to glass with refractive indices around 1.5. For high refractive index substrates, the use of gold nanocones may be restricted to longer wavelengths.

4.2 | Nanocone termination

The termination of metal nanocones onto the larger AFM cantilever has been shown to affect the near-field enhancement, with an increased refractive index red-shifting near-field enhancement.^[33] Figure 7 compares the near-field enhancement spectra for a gold-coated tip that forms a cap and a gold nanocone. The cap structure results in a 30% greater peak enhancement and a resonance that is blueshifted 15 nm. Given the significant increase in computation time when including the silicon structure and the small wavelength shift, free-standing metal nanocones were considered in this work.

4.3 | Tip-sample separation

In this section, the effects of tip-sample separation are investigated in terms of enhancement, location of spectral peaks and the spot size for nanocone tips.

Figure 8a shows the enhancement spectra for a nanocones, calculated 1 nm below the tip apex, at multiple tip-sample separations. As the sample is brought closer to the tip, the strongest spectral peak is redshifted and increases in amplitude. This effect is further explored in Figure 8b, which shows the enhancement as a

TABLE 1 Recommended nanocone material, length and cone angle combinations for common wavelengths in near-field lithography (785 nm) and tip-enhanced Raman spectroscopy (TERS) (633 and 514 nm) given a radius of 10 nm

Wavelength (nm)	Material	Angle (°)	Length (nm)	Enhancement
785	Gold	20	210	45
		30	275	34
633	Silver	20	160	54
		30	195	42
514	Gold	20	110	45
		30	155	35
514	Silver	20	95	54
		30	135	42

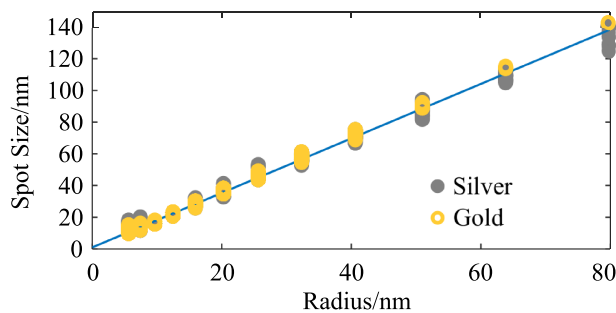


FIGURE 6 Near-field spot size (FWHM) as a function of radius for gold and silver nanocones. The spot size is measured 1 nm below apex with each data point representing a unique nanocone geometry. The radius is observed to be the dominant determinant of spot size. The linear fit is spot size (nm) = $1.72r(\text{nm}) + 1 \text{ nm}$

function of tip-sample separation 1 nm below the tip apex and at the sample surface. As the tip-sample separation increases, the enhancement below the tip apex decreases asymptotically towards the enhancement seen when there is no sample present. The enhancement at the sample surface decays towards 1 as the tip-sample separation increases, a trend consistent with experimental results.^[24,34-38] This shows that a small tip-sample separation increases the enhancement at the sample through two mechanisms. First and most significant, the sample being closer to the tip decreases the distance over which the evanescent field can decay. Second, there is an amplification of the near-field enhancement, which is evident as the enhancement measured at the tip apex increases when the tip-sample separation is decreased. This is due to the formation of a tip image in the substrate, increasing the dipole strength.^[32] Thus, for enhancement and resolution, the tip-sample separation should be minimised. Figure 8c shows that spot size increases linearly as a function of tip-sample separation from 0 to 30 nm typical in TERS. This is consistent with previous

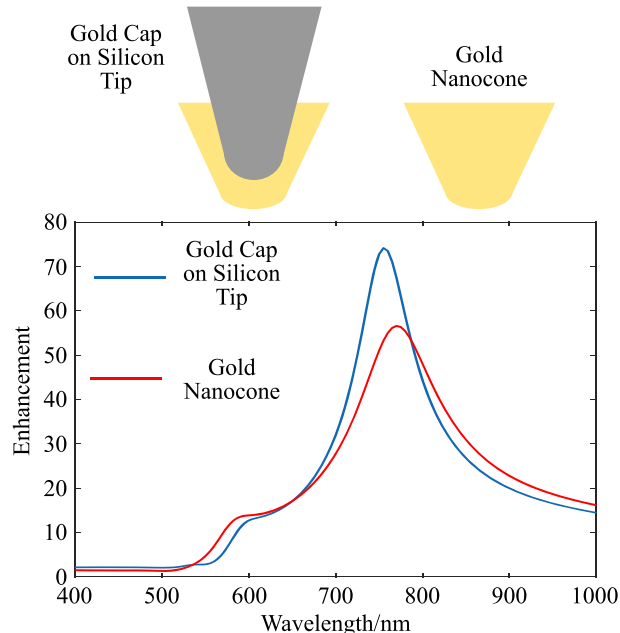


FIGURE 7 Near-field spectra for a gold-coated silicon tip apex (cap) and gold nanocone. The gold cones are both 250 nm long with a radius of curvature of 10 nm and a cone angle of 10°

work.^[6] Thus, for high enhancement and resolution, the tip-sample separation should be minimised.

4.4 | Future work

In future work, a range of nanocone geometries will be produced for specific excitation wavelengths, including 785 and 633 nm. The geometries of the nanocones will be selected based on the LSPR wavelength and enhancement models, given in Equations (1) and (2), respectively. A possible production method using focussed ion beam etching is described in the literature.^[3] Simulations also reveal the possibility of isolating a metal cap on a

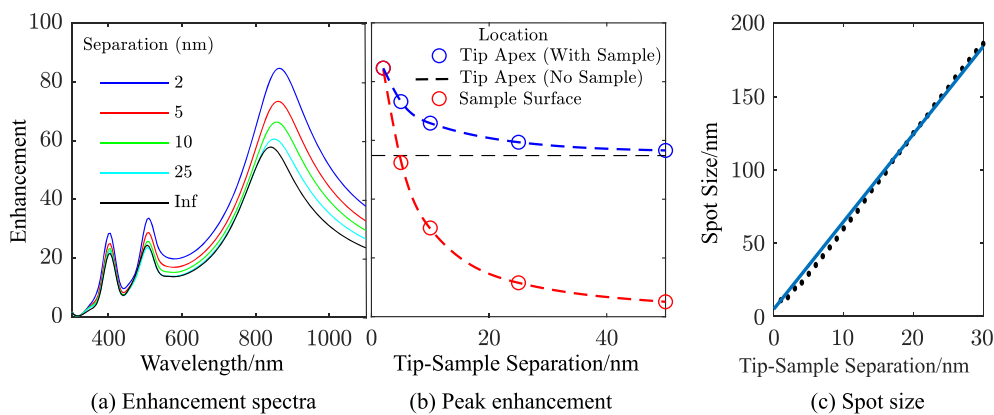


FIGURE 8 The effects of increasing tip-sample separation for a 250-nm silver nanocone with a radius of 10 nm and an angle of 10°, for (a) electric field enhancement spectra. (b) Electric field enhancement as measured 1 nm below tip apex (blue), 1 nm below the sample surface (red) and with the no sample (infinite tip-sample separation) case included as a reference (black). (c) The near-field spot size measured 1 nm below the sample surface (FWHM). The linear fit in (c) approximates the dependence of spot size on tip-sample separation

metal-coated AFM tip by etching a ring with a height of approximately 50 nm.^[33] The performance of the produced nanocones will be assessed with an emphasis on their applicability for TERS in terms of Raman signal enhancement and topographic resolution.

5 | CONCLUSION

This article describes a numerical method for optimising the enhancement and resonant wavelength of metallic nanocones for applications such as TERS. The BEM is utilised to simulate the optical response of a large number of metallic nanocones with unique combinations of length, half-angle and radius. Tip-sample separation is also considered. The materials of interest are gold and silver; however, the presented method is applicable to any metal.

The results show well-defined trends between each geometry parameter and the resulting resonance wavelength and tip-enhancement. Empirical functions are fitted to simulation results that describe the major trends. These empirical functions are useful for predicting performance and determining the optimal geometry for a given application.

For TERS, gold nanocones are found to have similar near-field enhancement to silver nanocones at red and near-infrared wavelengths. This is significant as gold has far superior corrosion resistance to silver, which could potentially increase the probe lifetime from hours, to days or weeks. However, gold nanocones do not provide competitive enhancement below 633 nm, so silver nanocones expected to be a better choice for applications requiring these wavelengths. This work highlights that the choice of material is strongly dependent on the required

operating wavelength. Nanocones are also predicted to have significantly improved resolution compared with metal-coated tips due to the smaller tip radius.

Future work includes fabrication of the optimal nanocone geometries and experimental validation of the simulation results. If successful, this is expected to lead to a new class of probes for TERS that provide simultaneously improved optical resolution, enhancement and topographical resolution.

ORCID

Luke R. McCourt <https://orcid.org/0000-0003-0593-6054>

Sathish C. Indirathankam <https://orcid.org/0000-0002-0180-8613>

REFERENCES

- [1] M. G. Ruppert, B. S. Routley, L. R. McCourt, Y. K. Yong, A. J. Fleming, Manuscript in preparation **2020**.
- [2] M. McMahon, R. Lopez, H. Meyer, L. Feldman, R. Haglund, *Appl. Phys. B* **2005**, *80*, 7.
- [3] M. Fleischer, A. Weber-Bargioni, M. V. P. Altoe, A. M. Schwartzberg, P. J. Schuck, S. Cabrini, D. P. Kern, *ACS Nano* **2011**, *5*, 4.
- [4] C. Girard, A. Dereux, *Rep. Prog. Phys.* **1996**, *59*, 5.
- [5] H. Furukawa, S. Kawata, *Opt. Commun.* **1998**, *148*, 4.
- [6] F. Festy, A. Demming, D. Richards, *Ultramicroscopy* **2004**, *100*, 3.
- [7] M. Pelton, G. W. Bryant, Surface Enhanced Raman Scattering, *Introduction to Metal-Nanoparticle Plasmonics*, Vol. 5, John Wiley & Sons **2013**, 233.
- [8] A. Hartschuh, N. Anderson, L. Novotny, *J. Microsc.* **2003**, *210*, 3.
- [9] R. M. Stöckle, Y. D. Suh, V. Deckert, R. Zenobi, *Chem. Phys. Lett.* **2000**, *318*, 1.
- [10] M. G. Ruppert, S. I. Moore, M. Zawierta, A. J. Fleming, G. Putrino, Y. K. Yong, *Nanotechnology* **2019**, *30*, 8.

- [11] X. Yin, N. Fang, X. Zhang, I. B. Martini, B. J. Schwartz, *Appl. Phys. Lett.* **2002**, *81*, 19.
- [12] O. T. Ghalehbeygi, A. G. Wills, B. S. Routley, A. J. Fleming, *J. Micro/Nanolithogr., MEMS, MOEMS* **2017**, *16*, 3.
- [13] B. J. Wiley, S. H. Im, Z.-Y. Li, J. McLellan, A. Siekkinen, Y. Xia, *J. Phys. Chem. B* **2006**, *110*, 32.
- [14] T.-X. Huang, C.-W. Li, L.-K. Yang, J.-F. Zhu, X. Yao, C. Liu, K.-Q. Lin, Z.-C. Zeng, S.-S. Wu, X. Wang, F.-Z. Yang, B. Ren, *Nanoscale* **2018**, *10*, 9.
- [15] P. R. Brejna, P. R. Griffiths, *Appl. Spectrosc.* **2010**, *64*, 5.
- [16] Y. Fujita, P. Walke, S. De Feyter, H. Uji-i, *Jpn. J. Appl. Phys.* **2016**, *55*, 8S1.
- [17] J. T. Krug, E. J. Sánchez, X. S. Xie, *J. Chem. Phys.* **2002**, *116*, 24.
- [18] K. Crozier, A. Sundaramurthy, G. Kino, C. Quate, *Appl. Phys.* **2003**, *94*, 7.
- [19] A. Haidary, Y. Miyahara, P. Grütter, COMSOL Conference **2014** (Boston).
- [20] M. Micic, N. Klymyshyn, Y. D. Suh, H. P. Lu, *J. Phys. Chem. B* **2003**, *107*, 7.
- [21] K. Lee, M. A. El-Sayed, *J. Phys. Chem. B* **2006**, *110*, 39.
- [22] A. Mohammadi, F. Kaminski, V. Sandoghdar, M. Agio, *J. Phys. Chem. C* **2010**, *114*, 16.
- [23] C. Schäfer, D. A. Gollmer, A. Horrer, J. Fulmes, A. Weber-Bargioni, S. Cabrini, P. James Schuck, D. P. Kern, M. Fleischer, *Nanoscale* **2013**, *5*, 17.
- [24] R. M. Roth, N. C. Panoiu, M. M. Adams, R. M. Osgood, C. C. Neacsu, M. B. Raschke, *Opt. Express* **2006**, *14*, 7.
- [25] U. Hohenester, A. Trügler, *Comput. Phys. Commun.* **2012**, *183*, 2.
- [26] J. Waxenegger, A. Trügler, U. Hohenester, *Comput. Phys. Commun.* **2015**, *193*, 138.
- [27] P. B. Johnson, R. W. Christy, *Phys. Rev. B* **1972**, *6*, 12.
- [28] Y. C. Martin, H. F. Hamann, H. K. Wickramasinghe, *Appl. Phys.* **2001**, *89*, 10.
- [29] N. Hayazawa, Y. Inouye, Z. Sekkat, S. Kawata, *Chem. Phys. Lett.* **2001**, *335*, 5.
- [30] G. W. Bryant, F. J. García de Abajo, J. Aizpurua, *Nano Lett.* **2008**, *8*, 2.
- [31] A. L. Demming, F. Festy, D. Richards, *J. Chem. Phys.* **2005**, *122*, 18.
- [32] A. Downes, D. Salter, A. Elfick, *J. Phys. Chem. B* **2006**, *110*, 13.
- [33] R. J. Hermann, M. J. Gordon, *Opt. Express, OE* **2018**, *26*, 21.
- [34] A. Hartschuh, E. J. Sánchez, X. S. Xie, L. Novotny, *Phys. Rev. Lett.* **2003**, *90*, 9.
- [35] B. Pettinger, K. F. Domke, D. Zhang, R. Schuster, G. Ertl, *Phys. Rev. B* **2007**, *76*, 11.
- [36] M. B. Raschke, C. Lienau, *Appl. Phys. Lett.* **2003**, *83*, 24.
- [37] T.-A. Yano, T. Ichimura, A. Taguchi, N. Hayazawa, P. Verma, Y. Inouye, S. Kawata, *Appl. Phys. Lett.* **2007**, *91*, 12.
- [38] J. Yu, Y. Saito, T. Ichimura, S. Kawata, P. Verma, *Appl. Phys. Lett.* **2013**, *102*, 12.

SUPPORTING INFORMATION

Additional supporting information may be found online in the Supporting Information section at the end of this article.

How to cite this article: McCourt LR, Ruppert MG, Routley BS, Indirathankam SC, Fleming AF. A comparison of gold and silver nanocones and geometry optimisation for tip-enhanced microscopy. *J Raman Spectrosc.* 2020; 1–9. <https://doi.org/10.1002/jrs.5987>